Renewable Energy xxx (2017) 1–14

Contents lists available at ScienceDirect

Renewable Energy

journal homepage: www.elsevier.com/locate/renene

Vibration-based bearing fault detection for operations and maintenance cost reduction in wind energy

Cédric Peeters*, Patrick Guillaume, Jan Helsen

Vrije Universiteit Brussel, Department of Mechanical Engineering, Pleinlaan 2, Elsene 1050, Belgium

ARTICLE INFO

Article history:
Received 1 September 2016
Received in revised form
17 January 2017
Accepted 24 January 2017
Available online xxx

Keywords:
Cepstrum
Editing
Whitening
Bearing fault
Deterministic/random separation

ABSTRACT

Critical mechanical faults in wind turbine systems lead to considerable downtime and repair costs. Improving the detection and diagnosis of such faults thus brings about significant cost reductions for operations and maintenance (O&M) and electricity production. One of the most common defects in drivetrains are rolling element bearing faults. Detecting the faults in their incipient phase can prevent a more catastrophic breakdown and save a company time and money. This paper focuses on separating the bearing fault signals from masking signals coming from drivetrain elements like gears or shafts. The separation is based on the assumption that signal components of gears or shafts are deterministic and appear as clear peaks in the frequency spectrum, whereas bearing signals are stochastic due to random jitter on their fundamental period and can be classified as cyclostationary. A technique that recently gained more attention for separating these two types of signals is the cepstral editing procedure and it is investigated further in this paper as an automated procedure. The performance of the developed methods is validated on experimental data from the National Renewable Energy Laboratory (NREL) in the context of the wind turbine gearbox condition monitoring round robin study.

1. Introduction

Wind turbines are exposed to strong dynamic excitation events such as varying wind speeds, electricity grid events, or sea waves (for offshore wind turbines) [1]. The production cost of electricity by wind turbines is strongly influenced by the reliability of the wind turbine systems [2]. The downtime and repair costs significantly contribute to the economic impact of faults. In particular gearboxes in wind turbines exhibit substantial downtime in case of failure [3] and bearings turn out to be the most critical component in wind turbine gearboxes [4,5]. In general, rolling element bearings are one of the most used components in wind turbine drivetrains. According to the statistics provided by the NREL gearbox reliability database, more than half (76%) of wind turbine gearbox failures are caused by bearings, with gear faults being the second major cause for failure (17.1%). It is estimated that overall more than 90% of all rotating machines [6] contain rolling element bearings. Unfortunately, they are susceptible to a multitude of premature deficiencies and less than 10% of rolling element bearings reach their expected basic L10 life, the life at which ten percent of the bearings can be expected to have failed due to normal fatigue failure for that particular application. These observations imply a need for an improved comprehensive condition-based maintenance program. However, there are still some hurdles to be overcome before such an exhaustive program becomes fully feasible. One of these problems is the detection of characteristic bearing fault frequencies that are masked by high energy harmonic signals originating from other machine elements like shafts or gears. Separating the bearing fault signals from other masking signal content of such elements is thus a valuable endeavor. The separation is based on the assumption that bearing fault signals are stochastic due to random jitter on their fundamental period and can be categorized as cyclostationary whereas gear or shaft signals are deterministic and appear as distinct peaks in the amplitude spectrum. An important factor to the success of a method is its robustness to noise. In addition to removing harmonic content, the method should not decrease the signal-to-noise ratio of potential faults [7,8].

Recently there have been a number of developments concerning the topic of discrete components removal (DCR). Time-synchronous averaging (TSA) [9] is a well-known technique primarily used when deterministic signal components are the main

* Corresponding author.
E-mail addresses: cedric.peeters@vub.ac.be (C. Peeters), patrick.guillaume@vub.ac.be (P. Guillaume), jahelsen@vub.ac.be (J. Helsen).

http://dx.doi.org/10.1016/j.renene.2017.01.056
0960-1481/

interest. It essentially averages over all the fundamental periods of a specific shaft or gear in a signal, producing a clean averaged vibration signal of one period of the component. However, it can also be used for deterministic component removal. By removing all of the obtained averaged deterministic signals, the residual signal consists mainly out of stochastic signal content.

Another method frequently used for discrete component removal is the self-adaptive noise cancellation method (SANC) [10]. This method is an adaptation of adaptive noise cancellation (ANC) which uses an adaptive filter to remove corresponding components between two signals mixed in a primary signal based on a reference signal. The SANC method replaces the reference signal with a slightly delayed version of the primary signal. This constitutes the removal of the deterministic components and produces a residual signal, retaining the stochastic content. A method based on the same approach as the SANC technique was developed by Antoni & Randall [10] and was called the discrete/random separation technique (DRS). A transfer function is calculated between the input signal and its delayed version. This transfer function filters out the deterministic content by fast convolution in the frequency domain.

An alternative approach is to model the deterministic components using past values of the vibration signal. By subtracting the predictable signal model from the full signal, the stochastic unpredictable signal content is obtained. This method is called linear prediction filtering (LPF) [11].

A more recent technique edits the real cepstrum [12] for the purpose of discrete component removal. It is this preprocessing technique that is investigated further in this paper as it shows great potential in separating cyclostationary bearing signals from discrete components. Qualitative studies conducted by Kilundu et al. [13] and Randall et al. [12] compare cepstral editing to the other aforementioned methods. These studies indicate through experimental tests that the cepstrum editing procedure (CEP) can outperform the other methods.

The aforementioned techniques have proven their worth in the past, but they have their disadvantages and the cepstral editing procedure also provides some advantages that the other methods lack. The TSA method, for example, requires the application of the TSA method for every different shaft or gear, making this process quite laborious. Afterward, the signal has to be reverted back from the angular domain to the time domain. The TSA method only removes harmonics of the signal and does not eliminate their modulation sidebands. It also modifies the full spectrum and cannot be performed for certain frequency bands only. When using linear prediction filtering for removal of discrete frequency content, one has to take care when choosing the model order. The order has to be smaller than the bearing fault impulse spacing and should maximize the impulsiveness of the residual signal. Sometimes criteria such as the Akaike Information criterion is used for selecting the optimum model order. Since both the SANC and DRS method are based on the same approach they have similar drawbacks. They both require the discrete signal components to have longer correlation lengths than the used delay, while the stochastic bearing signal content is assumed to have a short correlation length. These assumptions can limit the practical use of these methods for complex machinery. They also might treat low-frequency harmonics belonging to the bearing signal as discrete signal content and filter them out mistakenly. The cepstrum editing procedure (CEP) has the advantage that it is able to selectively remove certain harmonics by editing the corresponding components in the real cepstrum. This is a fairly straightforward operation and can tolerate some speed variation making order tracking often unnecessary. It can also remove modulation sidebands and operate on a smaller frequency band instead of the full spectrum. Lastly, it also does not require any filter optimization, iterative process or model order choices.

The ambition of this paper is to validate the performance of the cepstrum editing procedure by applying it to the well-documented experimental vibration data, provided by the *National Renewable Energy Laboratory* in light of a past *wind turbine gearbox condition monitoring round robin study*. While the cepstrum editing procedure takes care of the discrete/random separation, a number of other processing methods are applied to alleviate some other problems and enhance the fault detection. More in particular, order tracking, band-pass filtering, and envelope analysis are utilized as well. Inspection of the results indicates that the cepstrum editing procedure performs well in removing masking high-energy discrete frequency components from experimental vibration data. Cepstrum editing can thus prove to be a useful pre-processing tool before envelope analysis and can be easily included in extensive condition monitoring schemes [14].

The structure of this paper is as follows: Section 2 discusses the main processing methods used in this study. Section 3 provides details regarding the general characteristics of the test setup and the installed wind turbine components like the gearbox and bearings. Section 4 examines the results for the observable bearing faults. Finally, section 5 discusses the found results and conclusions.

2. Overview of the processing algorithms

Since the measured data originates from a complex machine, the full processing procedure consists of multiple steps. Fig. 1 shows a diagram containing the main processing stages used in this paper.

While NREL provides a tacho signal for the high-speed shaft (HSS) in the healthy measurements of the wind turbine gearbox, only a speed estimate in rotations per minute (RPM) is provided for the HSS data of the damaged gearbox. This means that an order tracking method is used for resampling the vibration in the angular domain based on extracting a virtual encoder signal (see Section 2.1).

The second processing step entails the separation of the vibration signal into deterministic signal components originating from the gears and shafts, and stochastic components coming from the bearings. A cepstrum editing procedure is used to attain this separation (see Section 2.2).

The third processing stage involves bandpass filtering the residual cepstrum edited signal in order to increase the bearing signal-to-noise ratio before demodulation (see Section 2.4). This step makes use of the kurtogram [15] and thus the optimal demodulation band is considered to be the frequency band with the highest kurtosis. The actual analysis of the data was performed both on the bandpass filtered data and on the unfiltered, full bandwidth data. Consequently, in some cases this processing step is not displayed when demodulating the full frequency band of the data showed higher values for the bearing fault frequencies.

The final processing stage calculates the squared envelope spectrum (SES) of the residual signal after cepstrum editing and bandpass filtering. Envelope analysis is probably one of the most used tools in bearing fault analysis and a lot of research has been done in the past improving the technique and understanding the full potential of it [16].

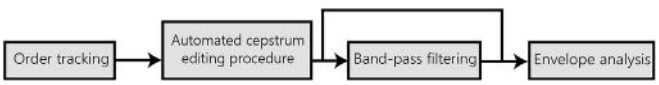

Fig. 1. Schematic diagram of the used processing steps.

Please cite this article in press as: C. Peeters, et al., Vibration-based bearing fault detection for operations and maintenance cost reduction in wind energy, Renewable Energy (2017), http://dx.doi.org/10.1016/j.renene.2017.01.056

2.1. Order tracking

In order to properly analyze the signals and to account for speed variation, the measured vibration signals need to be transformed from the time domain to the angular domain. Since the signals are sampled asynchronously with a constant sample rate, it is necessary to resample the signal at constant angular increments of a reference shaft. Usually, this is done based on rotation speed measurements from a tachometer, which can be used to estimate the angular shaft position. As previously mentioned, there is no available tacho signal for the damaged gearbox data. There are a number of ways in which to solve this absence of real tacho signal and to estimate the instantaneous angular speed (IAS), e.g. through Vold-Kalman filtering [17], a probabilistic approach [18], or simply bandpass filtering and counting the zero crossings [19]. If the estimated IAS is available, the signal can be resampled by interpolating the signal to obtain an angular domain signal instead of a time domain one. The angular resampling approach in this paper uses phase demodulation on the residual signal after bandpass filtering around a shaft harmonic.

2.2. Cepstrum editing procedure

2.2.1. The cepstrum

Throughout history, there have been various definitions and discussions of the cepstrum of a signal, the definitions used in this paper, however, are described as the complex and real cepstrum. The real cepstrum proves to be effective for achieving edited time signals by editing the logarithmic amplitude spectrum of stationary signals without having to fiddle with the phase.

Mathematically the complex cepstrum can be written as the inverse Fourier transform of the log spectrum, which is expressed in terms of the amplitude and phase:

$$C_c(\tau) = \mathscr{F}^{-1}\{log(X(f))\} = \mathscr{F}^{-1}\{ln(A(f)) + j\phi(f)\} \quad (1)$$

where $X(f)$ is the frequency spectrum of the signal $x(t)$:

$$X(f) = \mathscr{F}\{x(t)\} = A(f)e^{j\phi(f)}. \quad (2)$$

By setting the phase to zero in Eq. (1), the real cepstrum can be obtained:

$$C_r(\tau) = \mathscr{F}^{-1}\{ln(A(f))\}. \quad (3)$$

In Eq. (3) τ is referred to as *"quefrency"* and can be seen as a type of time-domain index. Harmonic components with a period h_0 in a signal correspond to a peak in the cepstrum at quefrency h_0.

2.2.2. Cepstral editing

The cepstrum has the interesting property that it is able to concentrate periodic spectral components (e.g. harmonics) into a smaller number of impulses called *"rahmonics"*. Removal of these peaks, also called *"liftering"*, corresponds to a decrease of the log amplitude of the periodic components in the signal. The complex cepstrum contains both amplitude and phase information which enables reversing back to time domain after editing, but in order to calculate the complex cepstrum the phase needs to be unwrapped. This is undesirable for stationary signals consisting of discrete frequency components, where the phase is undefined at intermediate frequencies [20].

However, it was recently shown by Randall & Sawalhi [21] that the real cepstrum is a more effective way of editing the log amplitude spectrum of signals containing harmonic components. Recombining this edited amplitude spectrum with the original phase produces the edited time domain signal. While the editing of certain frequencies introduces some phase distortion, this is generally negligible compared to the significant reduction in amplitude at those frequencies. A general scheme of the CEP method is shown in Fig. 2. It can be seen that the most crucial part in the CEP method is the editing of the real cepstrum. To enhance the applicability of the CEP method to industrial environments, an automated editing procedure is used in this paper instead of a manual one. It has been shown by Ompusunggu [22] that it is possible to implement a robust and efficient automated liftering of the harmonic signal content.

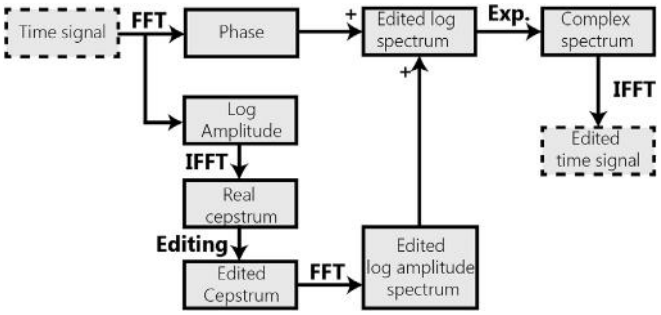

Fig. 2. Schematic diagram of the cepstrum editing procedure.

2.3. Automated cepstrum editing procedure (ACEP)

In order to replace the manual procedure by an automated one, there needs to be a more intelligent automated cepstral peak selection. Fig. 3 displays an overview of the steps to automate the editing. It can be seen that the real cepstrum is enhanced before the actual peak selection. The reason for the enhancement is simply to make the peak detection step easier and more straightforward. First, the cepstrum is long-pass liftered as to prevent liftering of low quefrency content. Second, a wavelet denoising and spectral subtraction (SS) method is used to reduce the amount of noise present in the signal. Afterward, a notch lifter is generated based on the automatic peak detection on the denoised cepstrum. Lastly, the original real cepstrum is liftered with the resulting notch lifter.

2.3.1. Long-pass lifter

Transforming the signal to the cepstral domain leads to a concentration of modal information in the low quefrency region. After the ACEP method however, the signal is bandpass filtered before envelope analysis, making it preferable to retain the system resonances. Thus, the low quefrency region is liftered away before the notch lifter generation step, implying that there are no detectable peaks corresponding to modal content.

If $n, N_{cut-off}$ and L are respectively the sample quefrency index, the cut-off quefrency index and the sample length of the cepstrum, the long-pass lifter can be defined as follows:

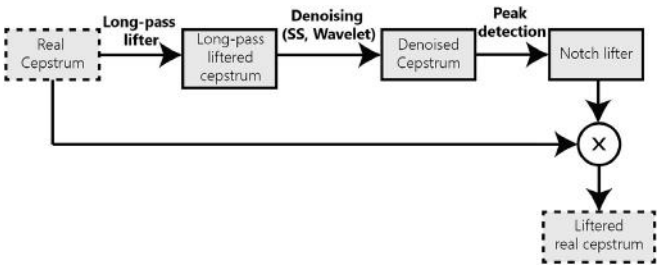

Fig. 3. Schematic diagram of the automated cepstrum editing step.

Please cite this article in press as: C. Peeters, et al., Vibration-based bearing fault detection for operations and maintenance cost reduction in wind energy, Renewable Energy (2017), http://dx.doi.org/10.1016/j.renene.2017.01.056

$$l_{LP}(n) = \begin{cases} 0 & n = 1 : N_{cut-off} \\ 1 & n = N_{cut-off} + 1 : L \end{cases} \quad (4)$$

Applying the lifter to the unedited real cepstrum $c(n)$ produces the long-pass liftered cepstrum:

$$c_{LP}(n) = c(n) l_{LP}(n). \quad (5)$$

2.3.2. Noise reduction

After the long-pass filtering step, the cepstrum is denoised using two conventional denoising methods. As proposed by Ompusunggu [22], the first applied method is spectral subtraction (SS). To smooth the cepstrum further, wavelet denoising is used afterward.

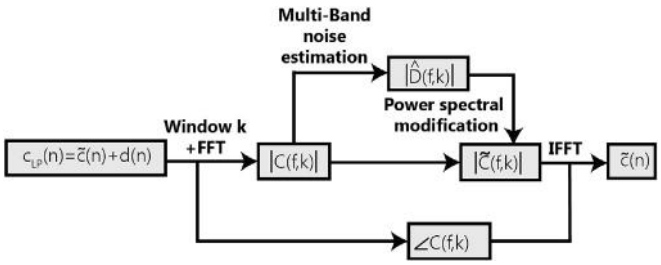

Fig. 4. Schematic diagram of the multi-band spectral subtraction method.

2.3.2.1. Spectral subtraction.

The spectral subtraction method was originally introduced as an acoustic speech enhancement technique and later an ample amount of variations have been developed [23]. In this paper, the multi-band spectral subtraction (MBSS) proposed by Kamath [24] is used.

The MBSS method estimates the noise spectrum and the average signal spectrum and then subtracts them from each other, improving the average signal-to-noise ratio (SNR). Usually, noise is colored and not perfect white Gaussian noise. The multi-band spectral subtraction method allows to some degree the presence of colored noise because the filtering of the signal spectrum is separated into different frequency bands.

Being a transformation of the measured time signal, the cepstrum contains noise as well and can be regarded as an addition of discrete signal components $\tilde{c}(n)$ and noise $d(n)$:

$$c_{LP}(n) = \tilde{c}(n) + d(n). \quad (6)$$

A diagram of the multi-band spectral subtraction technique is shown in Fig. 4. The SS technique makes use of a window basis for calculating the Fourier transform and performing the denoising procedure. The amplitude $|C(f,k)|$ is employed for estimating the average noise spectrum in every frequency band iteratively. The estimated amplitude $\left|\tilde{C}(f,k)\right|$ is obtained by subtracting the noise estimate from the original amplitude $|C(f,k)|$. Finally, the de-noised cepstrum $\tilde{c}(n)$ is reconstructed using the original phase $\angle C(f,k)$ and the amplitude estimates of all window frames.

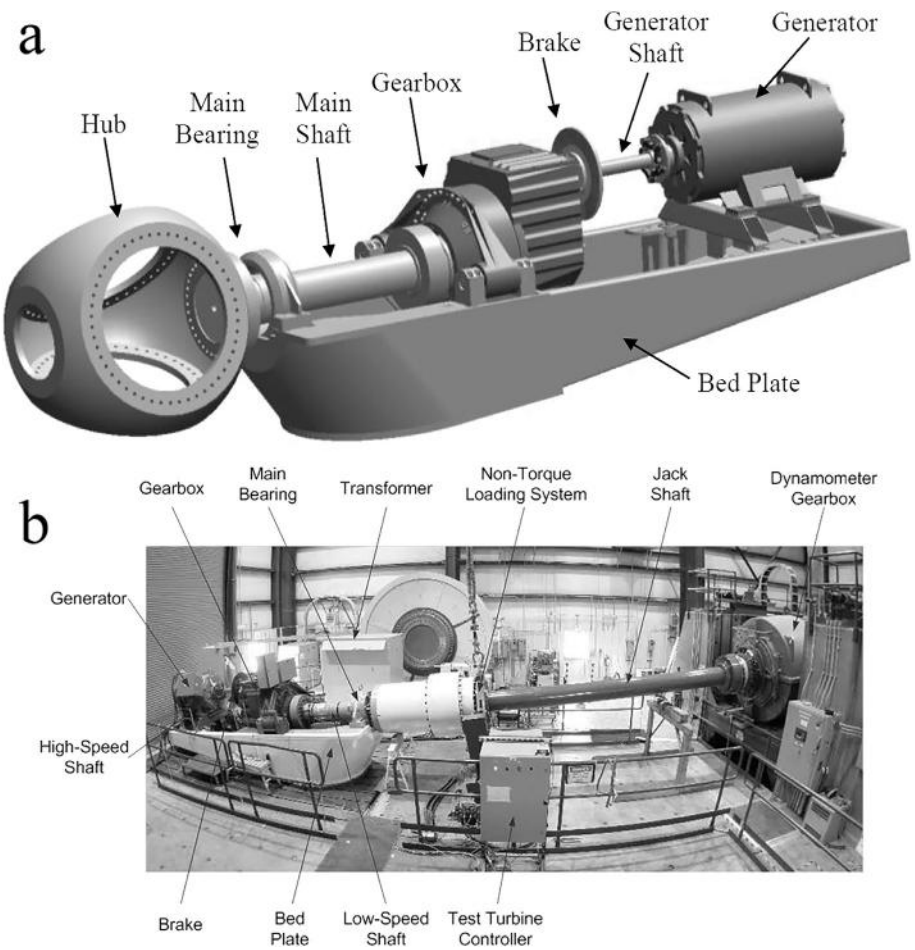

Fig. 5. (a) Drive train configuration of the test turbine. (b) NREL dynamometer test stand with the turbine installed.

Please cite this article in press as: C. Peeters, et al., Vibration-based bearing fault detection for operations and maintenance cost reduction in wind energy, Renewable Energy (2017), http://dx.doi.org/10.1016/j.renene.2017.01.056

2.3.2.2. Wavelet denoising. One of the primary applications of wavelets is denoising of signals. Wavelets allow for denoising in both time and frequency domain simultaneously and have even been used before as standalone method for bearing fault detection [25]. The wavelet denoising method described here makes use of Daubechies3 wavelets and of universal thresholding. This paper does not go further into detail about the used wavelet denoising method however.

2.3.3. Peak detection

After long-pass liftering and denoising, a fixed threshold of three standard deviations (3σ) is calculated from the residual cepstrum $c_r(n)$ as follows:

$$threshold = E[c_r(n)] + 3 \times std[c_r(n)], \tag{7}$$

where $E[.]$ and $std[.]$ denote respectively the expectation operator and the standard deviation operator. A vector m is constructed, based on all values greater than the threshold, containing all the corresponding sample indices:

$$m = \{\forall n | c_r(n) > threshold\} \tag{8}$$

While periodic signal components show up as sharp peaks in the cepstrum, second order cyclostationary components like bearing faults do not show up as a strong peak in the real cepstrum and thus they are not detected nor liftered away.

2.3.4. Liftering

The final editing step is the generation of the notch lifter, based on the cepstral peaks of the denoised cepstrum, and the actual liftering of the unaltered real cepstrum with this lifter. It should be noted however that the notch width has an influence on the performance of the ACEP method. If there is speed variation present in the signal, it can be desirable to choose a larger notch width, but it should not be chosen too large either since this can lead to excessively distorting the amplitude spectrum.

2.4. Bandpass filtering based on kurtosis & envelope analysis

This paper makes use of spectral kurtosis to identify appropriate frequency bands for demodulation. More in particular the kurtogram, developed by Jérôme Antoni [15], is utilized to visually determine impulsive frequency bands with high kurtosis values. For more information about the background and use of the kurtogram, the reader is referred to Ref. [15]. In this study, the envelope spectrum is used for the bearing fault frequency detection and is simply calculated by taking the Fourier transform of the squared modulus of the Hilbert transform of the vibration signal.

3. Experimental application

In order to test the performance of the developed methods, experimental data of a wind turbine from the National Renewable Energy Laboratory (NREL) will be used for validation and the results are compared to those summarized in Ref. [26]. In this report, a number of participating research partners published their findings [19,27–31] and these form a valuable background for this study. The NREL dynamometer test facility (DTF) was used for the data collection.

3.1. Description of experimental setup

3.1.1. Turbine

As can be seen on Fig. 5(a), the test turbine is a three-bladed, stall-controlled, upwind turbine. It has a rated power of 750 kW and the generator normally operates at 1800 rpm or 1200 rpm nominal. The complete drivetrain is installed in the NREL DTF as shown on Fig. 5(b). It is hard fixed to the floor and misses the hub, rotor, yaw bearing and yaw drives.

3.1.2. Gearbox

Two gearboxes of the same design are used for collecting the data, one in "healthy" state and the other one in "damaged" state. An exploded view of the gearbox is shown in Fig. 6(a). The accelerometer vibration measurements along with high-speed shaft RPM data was made available. The "healthy" gearbox is only tested in the dynamometer while the "damaged" gearbox did a run-in first in the dynamometer and was later sent to a wind farm for field testing. Two loss-of-oil events damaged its internal bearings and gears. Afterward, it was again installed in the dynamometer facility and retested in a controlled environment. The gearboxes consist of one low speed (LS) planetary stage and two parallel stages. The used nomenclature is the same as the one used by Sheng [26] and can be seen in Fig. 6(b).

3.1.3. Bearings

Various bearing types are used in the gearboxes corresponding to the loading conditions and life requirements. Two full-complement cylindrical roller bearings (fcCRB) support the planet carrier and two cylindrical roller bearings (CRB) support the planet gears. The parallel shafts are each supported by a CRB on the upwind side and by two tapered roller bearings (TRB) on the downwind side of the assembly. A list of all bearing locations, manufacturers, part numbers and types can be found in Table 1 and Fig. 7 illustrates the locations and used names of the different bearings. If the component is positioned upwind, this is

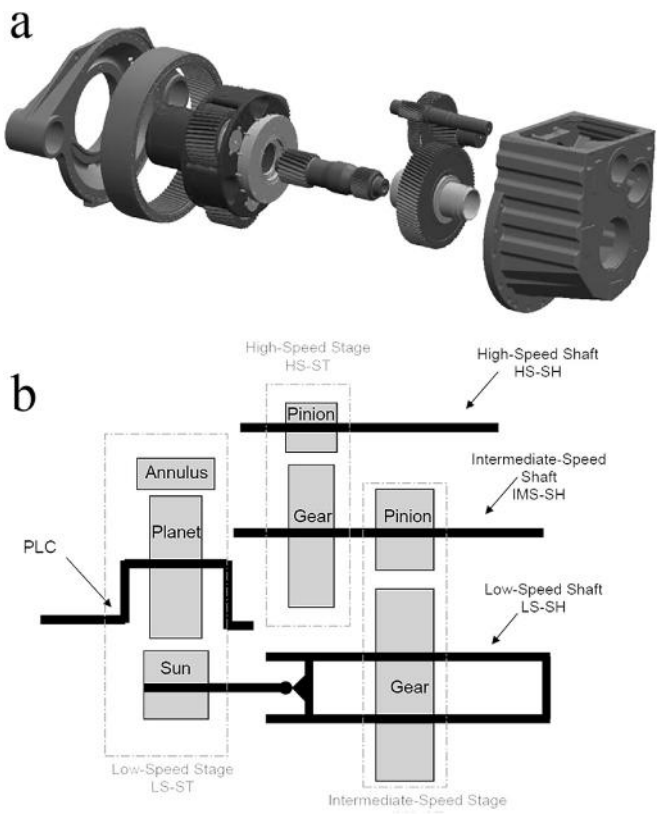

Fig. 6. (a) View of internal components of the test gearbox. (b) Internal nomenclature and abbreviations of the test gearbox.

Please cite this article in press as: C. Peeters, et al., Vibration-based bearing fault detection for operations and maintenance cost reduction in wind energy, Renewable Energy (2017), http://dx.doi.org/10.1016/j.renene.2017.01.056

Table 1
Overview of used bearing types, numbers and locations.

Location	Location designation	Type	Provider	Part number
Planet carrier	PLC-A	fcCRB	INA	SL181892E
	PLC-B	fcCRB	INA	SL 18 1880 72/K10
Planet	PL-A	CRB	FAG	NJ2232E.M1
	PL-B	CRB	FAG	NJ2232E.M1
Low-speed shaft	LS-SH-A	fcCRB	INA	SL181856E
	LS-SH-B	TRB	SKF	32948*
	LS-SH-C	TRB	SKF	32948*
Intermediate-speed shaft	IMS-SH-A	CRB	FAG	NU2220E.M1
	IMS-SH-B	TRB	SKF	32032 X
	IMS-SH-C	TRB	SKF	32032 X
High-speed shaft	HS-SH-A	CRB	FAG	NU2220E.M1
	HS-SH-B	TRB	SKF	32222 J2
	HS-SH-C	TRB	SKF	32222 J2

denoted with an 'A' and if it is downwind, with a 'B' or a 'C'. A full list of the gear and bearing characteristic frequencies is not given but can be determined based on Table 1.

3.2. Measurement settings

The accelerometers are mounted on the outside of the gearbox and data is sampled at 40 kHz per channel. In total data sets of eight accelerometers (Model: IMI 626B02) are made available and the exact locations can be seen in Fig. 8. Lastly, Table 2 gives a summary of the signal names and their corresponding locations of the different vibration sensors.

3.3. Performance analysis

In order to assess the performance of the developed methods for bearing fault detection, the provided signals at 1800 rpm from the NREL test setup are investigated using a combination of the above-mentioned techniques. This results in four basic steps:

1. Order tracking
2. Automated cepstral editing
3. Bandpass filtering based on kurtosis
4. Squared envelope analysis

According to the report of [26], the research partners of the *Wind Turbine Gearbox Condition Monitoring Round Robin Study* agreed to a total of seven damages that were considered to be

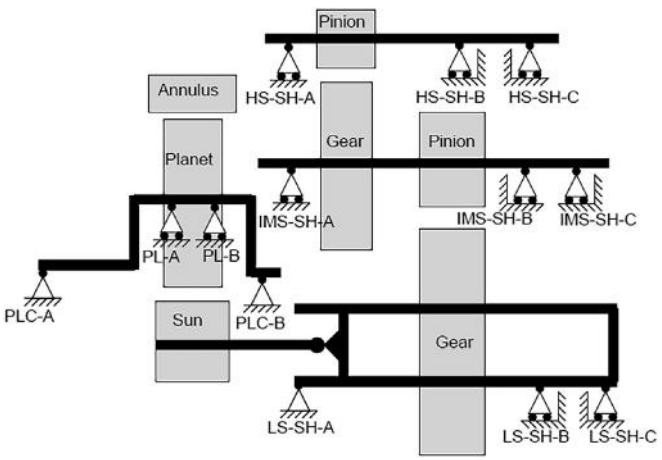

Fig. 7. Locations and nomenclature of the bearings in the test gearbox.

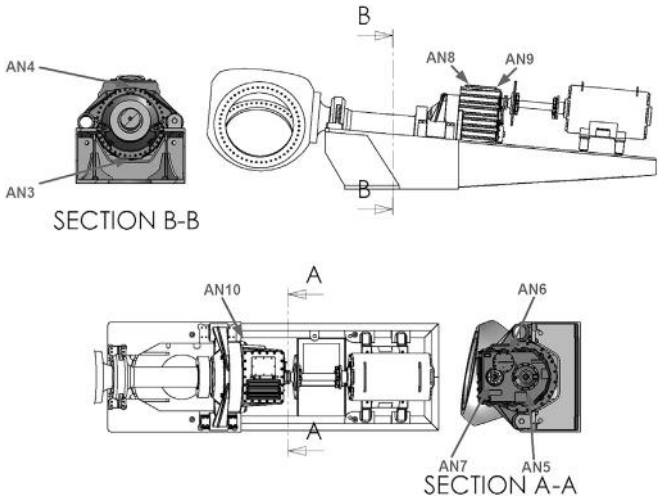

Fig. 8. Overview of the accelerometer locations.

Table 2
List of the used sensors and their corresponding placement descriptions.

Sensor label	Location description
AN3	Ring gear radial 6 o'clock
AN4	Ring gear radial 12 o'clock
AN5	LS-SH radial
AN6	IMS-SH radial
AN7	HS-SH radial
AN8	HS-SH upwind bearing radial
AN9	HS-SH downwind bearing radial
AN10	Carrier downwind radial

Table 3
Actual gearbox damage that should be detectable through vibration analysis.

Damage #	Component	Mode
1	HS-ST gear set	Scuffing
2	HS-SH downwind bearings	Overheating
3	IMS-ST gear set	Fretting corrosion, scuffing, polishing wear
4	IMS-SH upwind bearing	Assembly damage, scuffing, dents
5	IMS-SH downwind bearings	Assembly damage, dents
6	Annulus/ring gear, or sun pinion	Scuffing and polishing, fretting corrosion
7	Planet carrier upwind bearing	Fretting corrosion

detectable through vibration analysis. Table 3 shows a summary of the detectable gearbox damage.

Since this paper focuses on bearing fault detection, no attention is given to the gear faults, meaning that four bearing faults are investigated. For each bearing the characteristic frequencies corresponding to the damages are shown in Table 4.

Table 4
Damaged bearings and their corresponding theoretical characteristic frequencies. (BPFO: Ball Pass Frequency Outer race, BPFI: Ball Pass Frequency Inner race, FTF: Fundamental Train Frequency).

Bearing label	Fault type	Detectable characteristic frequency [Hz]
HS-SH downwind bearings (*HSS-B& C*)	BPFI FTF	345,29 Hz 12,75 Hz
IMS-SH downwind bearings (*ISS-B& C*)	BPFO	105,75 Hz
Planet carrier upwind bearing (*PLC-A*)	BPFO	8,81 Hz
IMS-SH upwind bearing (*ISS-A*)	BPFI	73,7 Hz

Please cite this article in press as: C. Peeters, et al., Vibration-based bearing fault detection for operations and maintenance cost reduction in wind energy, Renewable Energy (2017), http://dx.doi.org/10.1016/j.renene.2017.01.056

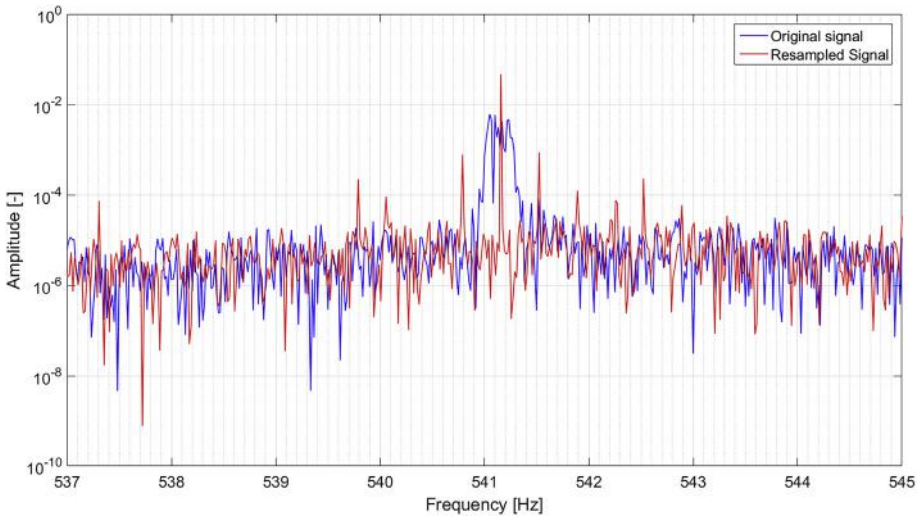

Fig. 9. Zoom of the 18th harmonic of the 30 Hz shaft speed, measured by the AN7 sensor for the damaged gearbox, before and after resampling.

4. Results

The bearing faults present in the system are spatially distributed over the gearbox, meaning that some sensors will be more likely to detect possible faults than others due to being in closer proximity to the source. To illustrate this and the used processing steps, the

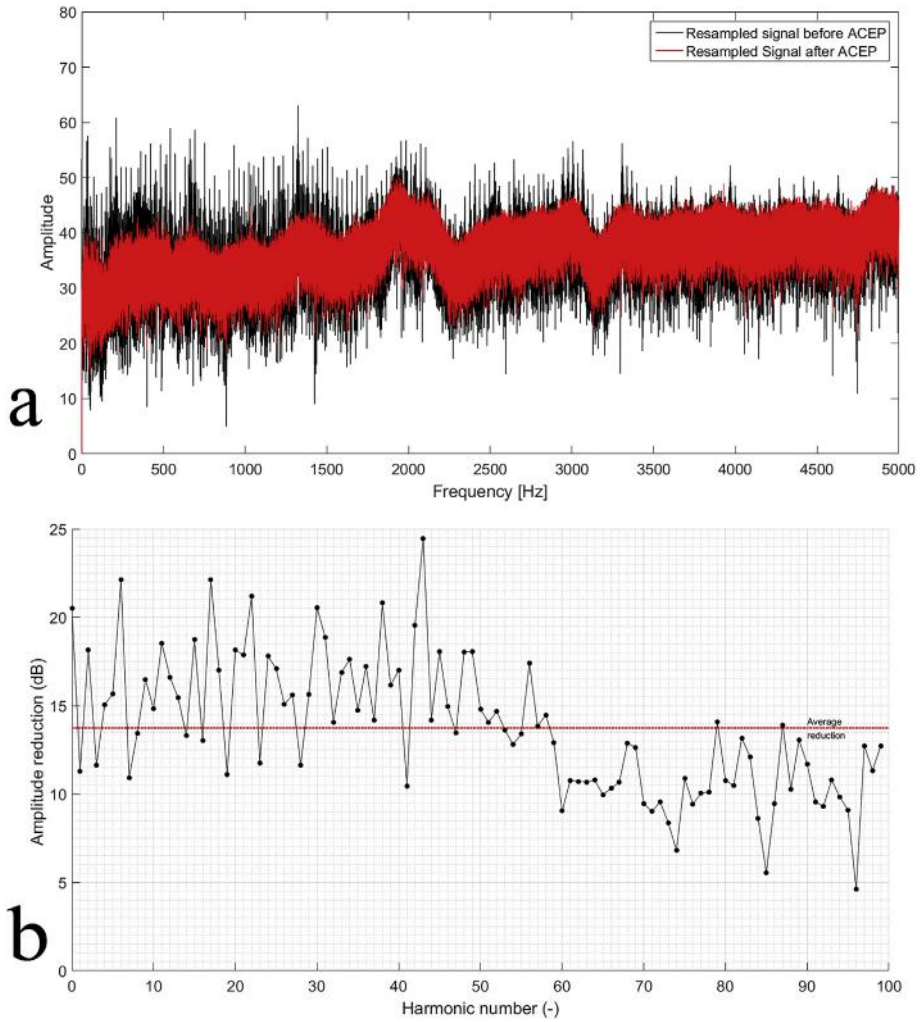

Fig. 10. (a) Amplitude spectrum of the AN7 sensor signal before and after ACEP. (b) Graph showing the amplitude reductions, in dB, of the first 100 shaft speed harmonics.

Please cite this article in press as: C. Peeters, et al., Vibration-based bearing fault detection for operations and maintenance cost reduction in wind energy, Renewable Energy (2017), http://dx.doi.org/10.1016/j.renene.2017.01.056

signal measured by sensor AN7 is analyzed. This sensor is located near the high-speed shaft bearings, so it is expected that it should contain prominent signal content originating from the BPFI and FTF faults described in Table 4.

4.1. High-speed downwind bearings

The first step in the processing scheme is to resample the healthy and the damaged data so the speed variation present in the measurements is neutralized. Using the provided tacho signal for the healthy signals, RPM measurements, and pseudo-encoder method (see Section 2.1)for the damaged signals, all the signals are resampled to provide a more accurate view on the frequencies present in the data. Fig. 9 shows a zoomed picture of the 18th shaft speed harmonic, around 540 Hz, before and after resampling of the damaged signal. It can be seen that the smearing of frequency peaks in the spectrum due to speed variation, is greatly reduced after resampling. Only one peak remains at a multiple of the fundamental shaft speed frequency.

Now that the frequencies in the spectrum are more pronounced, automatic cepstral editing is performed on the signal in order to remove the deterministic content of the resampled signal as much as possible. The ACEP method described in section 2.3 is used and the results on the spectrum of the damaged data of the AN7 sensor is shown in Fig. 10a. The damaged data exhibited very prominent shaft speed harmonics and due to the difficulty in properly displaying the total amount of reduction of harmonic content in a spectrum, a graph of the first 100 shaft speed harmonics is presented in Fig. 10b. It can be seen that the ACEP method performs well and is able to reduce these shaft speed peaks by an average of around 13 dB.

The residual signals after ACEP are now used for calculating the envelope spectra. The kurtograms of both the healthy and damaged data are generated and examined for differences. Fig. 11 displays the calculated kurtograms and here it can be seen that there is an increase in kurtosis around 13,2 kHz. First however, the normalized envelope spectra of the healthy and damaged data are examined without the use of the kurtogram, thus without bandpass filtering. The result of this can be seen in Fig. 12a. While the ACEP technique tries to reduce the influence of the shaft speed as much as possible, a prominent peak can still be seen at the high-speed shaft frequency ($1\times$ *HSS*) in the envelope spectrum. This is explained by the fact that ACEP only removes additive components and not modulating ones. Multiple peaks at harmonics of 345 Hz can be observed for the healthy as for the damaged data. The fundamental 345 Hz peak is close to the 2nd harmonic of the sun gear mesh frequency and the 46nd harmonic of the intermediate shaft speed frequency, but is not an exact multiple of one of these frequencies. Since this component is so prominently present after cepstral editing, it is concluded that the peak in the healthy and damaged data corresponds to the inner race defect frequency or BPFI of the high-speed downwind bearings, which is theoretically around 345.29 Hz for a shaft speed of 30 Hz. This is supported further by the presence of harmonics of the BPFI and side bands at 30 Hz in the envelope spectrum. Based on these envelope spectra, it appears though that the inner race damage was already present in the baseline healthy data.

While the gear faults are not the focus of this paper, it is noted that in Fig. 12a, the envelope spectrum displays a high value at 661 Hz for the damaged data. This corresponds to the gear mesh tooth passing frequency (*GMF*) of the intermediate-speed shaft (ISS) with the high-speed shaft. The damage report verified that the ISS gear exhibited corrosion, scuffing and wear.

The next analysis step makes use of bandpass filtering, based on the info portrayed by the kurtograms in Fig. 11. Fig. 12b shows a zoom of the envelope spectrum of the residual signal after bandpass filtering. Examination of the spectrum reveals a high peak

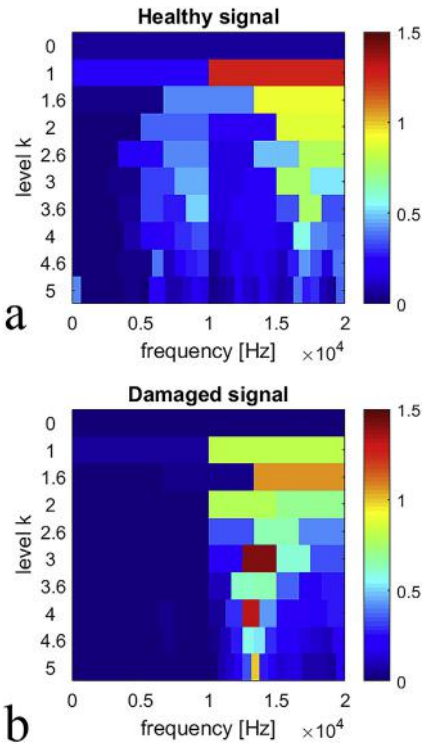

Fig. 11. (a) Kurtogram of the healthy AN7 sensor data. (b) Kurtogram of the damaged AN7 sensor data.

around 12.71 Hz, which corresponds to the fundamental train frequency (FTF) of the high-speed downwind bearings. Fig. 12b shows a clear increase of this frequency in the damaged data compared to the healthy data. Finally, as can be seen in Fig. 12a, the modulation by the 30 Hz shaft speed has increased significantly. This can indicate a possible high-speed shaft imbalance or misalignment or it can be associated with the BPFI modulation of the HSS-B&C bearings. However, the presence of imbalance was later corroborated by the damage report so it is most likely the combination of the two mentioned faults.

In order to demonstrate the effect of the ACEP procedure on the envelope spectrum, the damaged data is investigated before and after applying cepstral editing. Fig. 13a shows the envelope spectrum of the damaged data of the AN7 sensor before and after cepstral editing and without band-pass filtering. The spectrum before ACEP exhibits far more harmonic peaks, making it difficult to assess possible bearing faults. Added to this, these harmonics mask the presence of bearing faults, as is shown in Fig. 13b. The BPFI of the HSS downwind bearings cannot be detected here before cepstral editing.

4.2. Intermediate-speed shaft downwind bearings

The analysis procedure followed for the other bearings is similar to the one explained for the high-speed bearings. To reduce the number of figures, only the resulting envelope spectra are shown. As such, the analysis of the AN6 sensor, which is located close to the intermediate-speed shaft (ISS), is investigated for possible ISS bearing faults. After resampling and cepstral editing, the full-bandwidth envelope spectrum for the damaged case, shown in Fig. 14, exhibits clear peaks at even harmonics of the BPFO(105.25 Hz) of the ISS-B&C bearings. It does not however offer clear indications of the fundamental defect frequency itself. The kurtogram is used for determining the bandpass filter cut-off

Please cite this article in press as: C. Peeters, et al., Vibration-based bearing fault detection for operations and maintenance cost reduction in wind energy, Renewable Energy (2017), http://dx.doi.org/10.1016/j.renene.2017.01.056

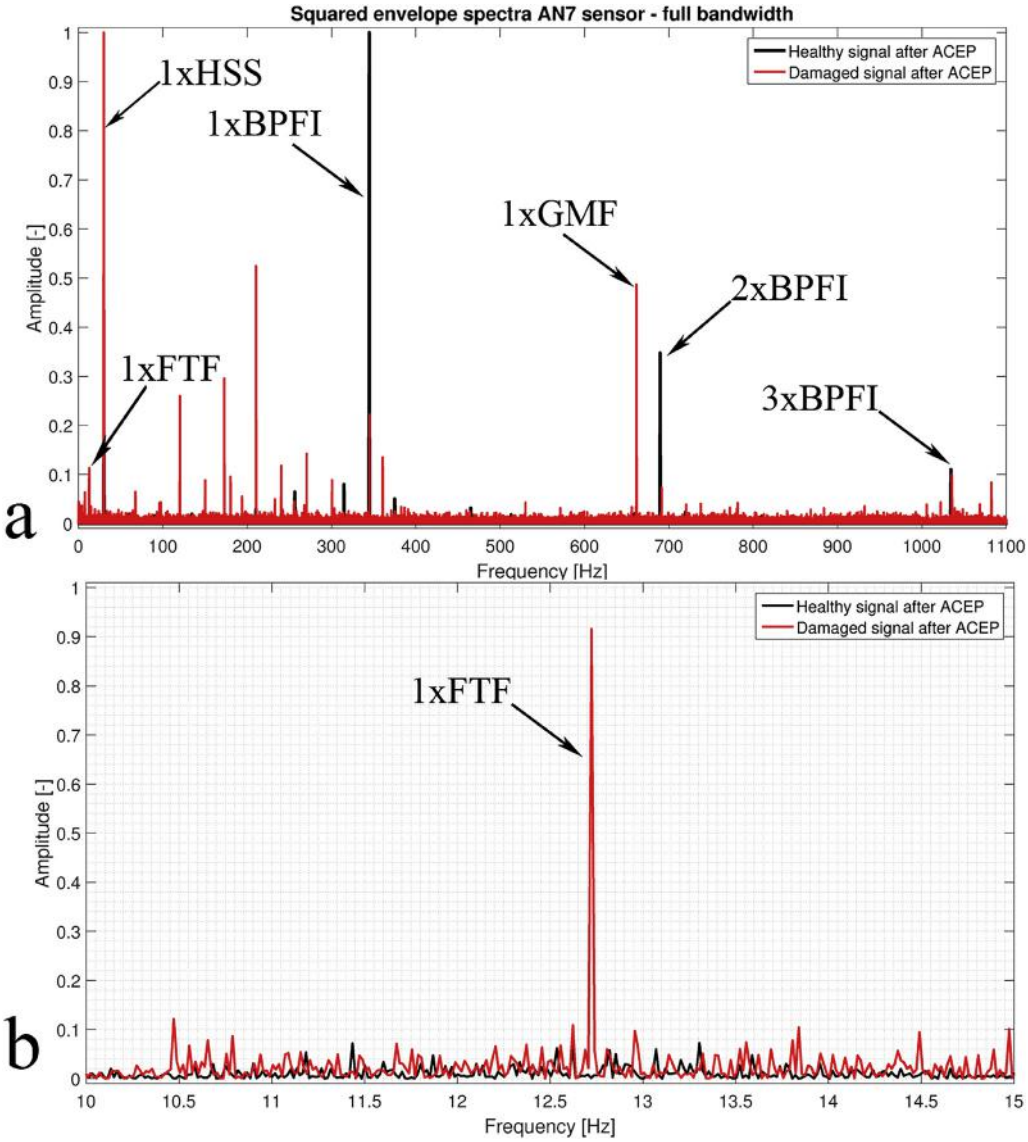

Fig. 12. (a) Envelope spectrum generated without the use of filters/kurtogram, indicating the presence of the BPFI & FTF of the high-speed downwind bearings (HSS-B&C). (b) Zoom of the envelope spectrum around the FTF frequency for the healthy and damaged signals after applying ACEP.

frequencies and is shown in Fig. 15. Using a bandpass filter centered at 16.4 kHz with a bandwidth of approximately 1 kHz produces the envelope spectrum of Fig. 16. This bandpass filter corresponds to the yellow rectangle in the kurtogram figure. In this envelope spectrum, the fundamental fault frequency is clearly revealed. However for the greater part of the full frequency band of the signal, mainly the even harmonics of the BPFO were discernable. This could imply that there are multiple point defects on the bearings, introducing cancellation and reinforcement of components which can modify the appearance of the envelope spectrum. The damage report confirms this and describes multiple dents, assembly damage and plastic deformation of the ISS downwind bearings. A zoom of the second BPFO harmonic at 210.4 Hz can be seen in Fig. 17 and illustrates the increase in amplitude of this frequency compared to the healthy case.

4.3. Intermediate-speed shaft upwind bearing

Damage was also reported for the ISS upwind bearing and evidence of this was found by using a bandpass filter with a center frequency of 10 kHz and bandwidth 1 kHz. The envelope spectrum in Fig. 18 exhibits a high peak at 72.94 Hz, which is close to the theoretical BPFI of 73.7 Hz for the ISS upwind bearing. The slight deviation of the theoretical value is likely due to slip of the roller elements. While this component is quite prominently present in the AN6 and AN7 data set, it is easily mistaken for the second harmonic of the gear mesh tooth passing frequency of the planet gears, which is 73.05 Hz. However, due to its presence after ACEP and the small frequency difference, it can be concluded that it is, in fact, the BPFI of the ISS upwind bearing.

4.4. Planet carrier upwind bearing

A similar approach as for the ISS-B& C bearings is used for detecting the 8,8 Hz outer race defect frequency of the planet carrier upwind bearing (PLC-A). A zoom of the full-bandwidth envelope spectrum is shown in Fig. 19. While the damage report does state that there was fretting corrosion present on the PLC upwind bearing, the corresponding frequency peaks are small and difficult to detect. The partners who participated in the wind turbine

Please cite this article in press as: C. Peeters, et al., Vibration-based bearing fault detection for operations and maintenance cost reduction in wind energy, Renewable Energy (2017), http://dx.doi.org/10.1016/j.renene.2017.01.056

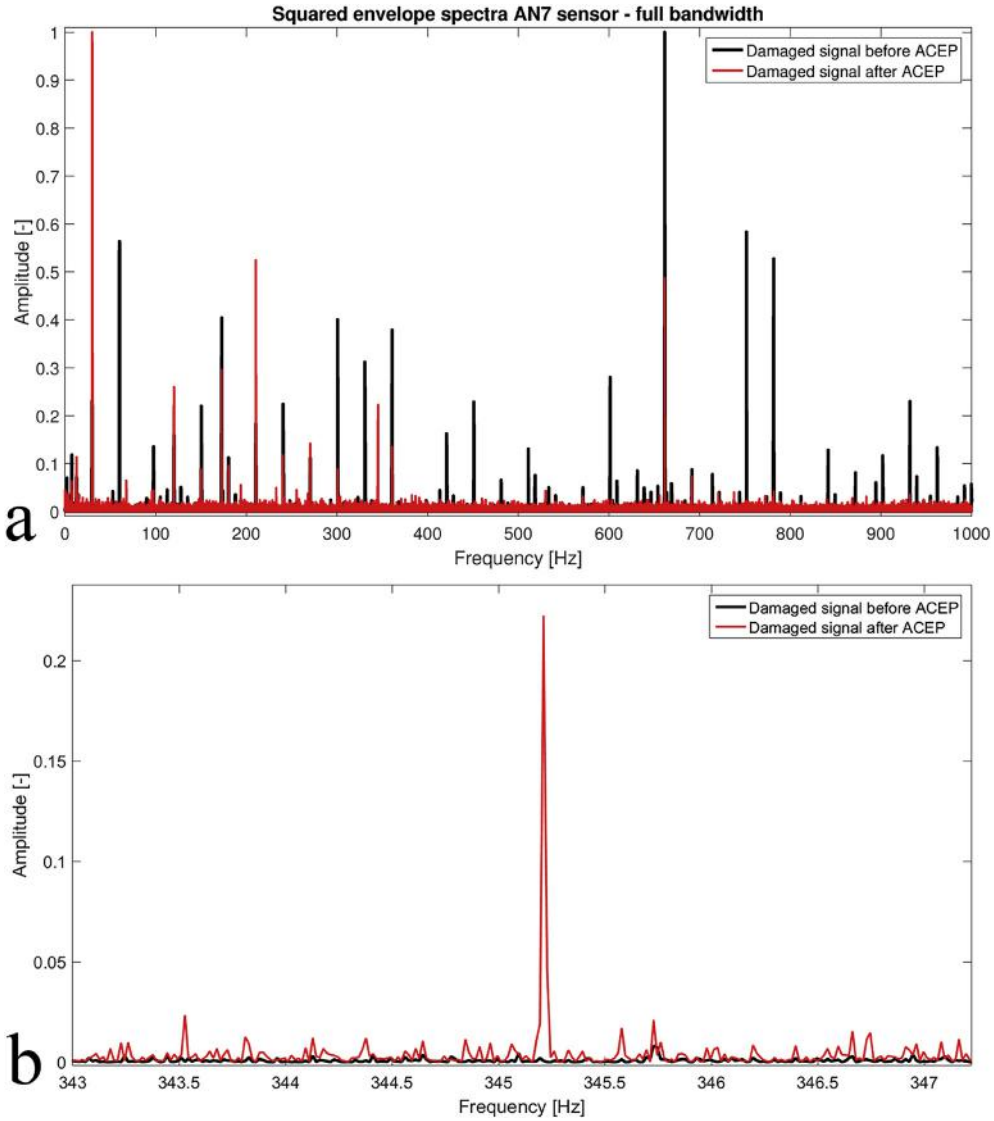

Fig. 13. (a) Envelope spectrum of damaged data before (*black line*) and after ACEP (*red line*). (b) Zoom of envelope spectrum around 345 Hz, the BPFI frequency of the high-speed downwind bearings, before and after ACEP. (For interpretation of the references to colour in this figure legend, the reader is referred to the web version of this article.)

gearbox condition monitoring round robin study confirmed this observation as well. Almost no one of the partners was successful in detecting this damage blindly and from Fig. 19a it can be understood why.

5. Results & discussion

In order to concisely summarize the findings of this study, the results of the bearing fault vibration analysis are presented again in Table 5. For four out of five faults, there are clear indications of the fault in the envelope spectra. Only the planet carrier upwind bearing showed no significant frequency peak no matter which demodulation band was chosen. This corresponds to the findings of other research partners that reported similar results. The planet carrier bearing fault was considered to be difficult to detect through standard vibration analysis, given the used measurement setup.

While the mentioned bearing frequencies are deemed detectable through vibration analysis, the fault frequencies originating from bearings mounted on the lower speed shafts are more difficult to detect than those on higher speed shaft, as can be expected. For example, the inner race fault frequency and the fundamental train frequency of the high-speed shaft downwind bearings are quite simple to detect, since these frequencies are already clearly visible in the full-bandwidth envelope spectrum after cepstrum editing. In contrast, the detection of the outer race fault frequency of the intermediate-speed shaft downwind bearings is a bit less straightforward due to the lack of a fundamental frequency peak in the full-bandwidth envelope. The even harmonics however show high envelope spectrum peaks, and after bandpass filtering, the fundamental frequency shows up in the analysis. Bandpass filtering around a specific center frequency is also required for the detection of the inner race fault of the intermediate-speed shaft upwind bearing. The planet carrier upwind bearing, which rotates at the lowest speed of all the mentioned bearings, was reported to have fretting corrosion, but did not exhibit any significant signs of actual damage in the vibration signals.

Although it is not the focus of this paper, high values for some of the gear fault frequencies are observed in the generated envelope spectra. A general remark (which others have stated as well) is that because of the presence of multiple progressed faults of gears and bearings, the analysis is encumbered due to the multitude of modulating components present in the envelope spectra. Most of

Please cite this article in press as: C. Peeters, et al., Vibration-based bearing fault detection for operations and maintenance cost reduction in wind energy, Renewable Energy (2017), http://dx.doi.org/10.1016/j.renene.2017.01.056

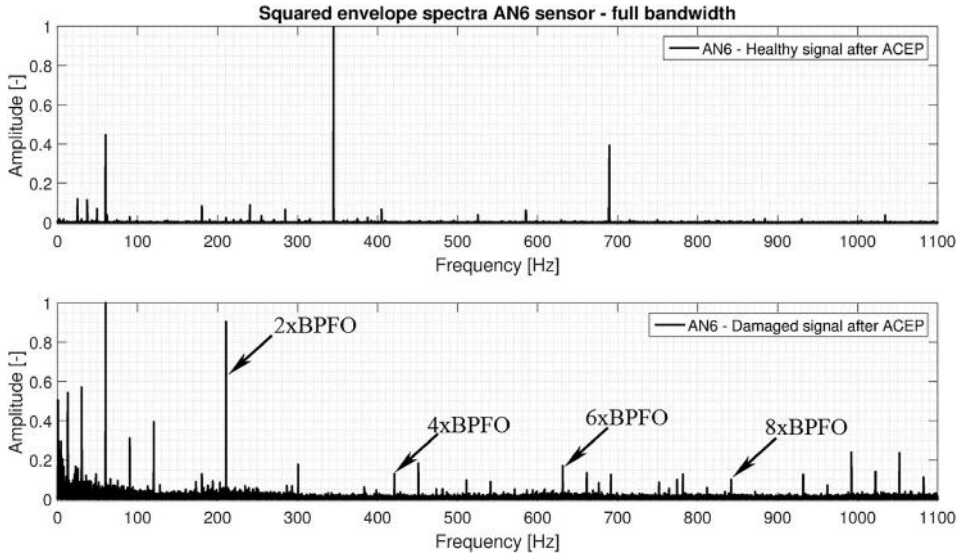

Fig. 14. Envelope spectrum of AN6 acceleration signal after resampling and ACEP for the healthy case (*above*) and damaged case (*below*).

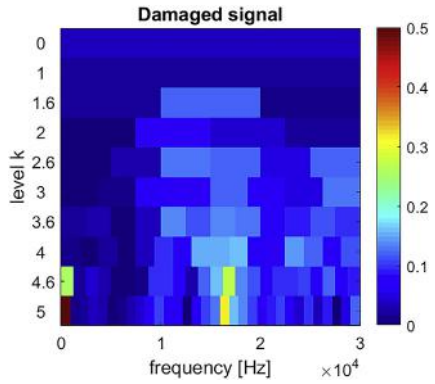

Fig. 15. Kurtogram of the AN6 signal after automated cepstrum editing.

the described faults produce second-order cyclostationary components which make it difficult to analyze them separately since the cepstrum editing procedure only filters out the deterministic components but leaves the cyclostationary components intact. Thorough visual inspection of the envelope spectra is thus necessary to attribute the fault frequencies to the correct envelope peaks.

Compared to other methods, the cepstrum editing procedure is well-suited for this application. The wind turbine contains a complex multi-stage gearbox, consisting of multiple shafts, which would make the removal of masking discrete frequency content by time synchronous averaging methods very time-consuming since every shaft's influence would have to be removed separately. Even then, modulation sidebands would still remain present in the vibration signal. Using linear prediction filtering based on autoregressive models also does not work properly for this particular case.

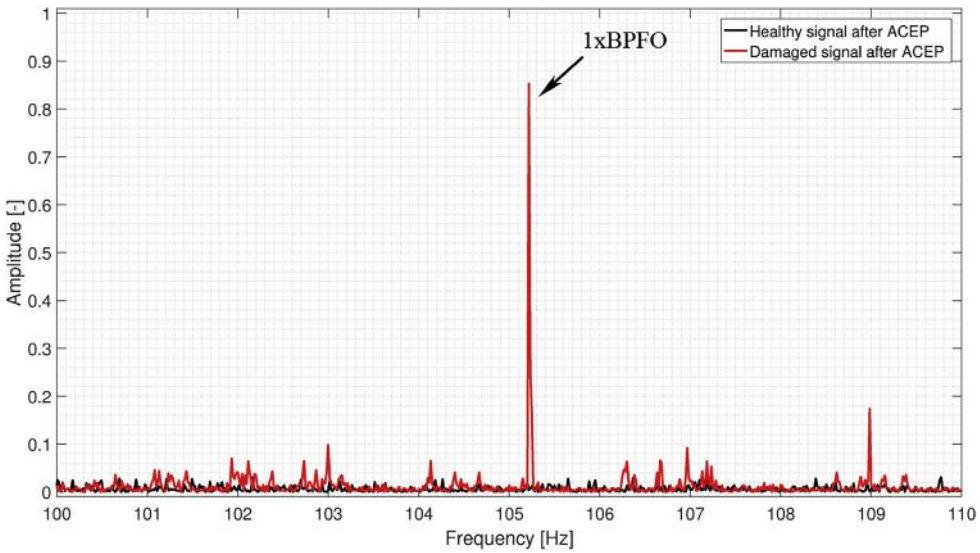

Fig. 16. Zoom of envelope spectrum of AN6 acceleration signal around the BPFO fundamental of the ISS-B&C bearings for the healthy case (*black*) and damaged case (*red*). (For interpretation of the references to colour in this figure legend, the reader is referred to the web version of this article.)

Please cite this article in press as: C. Peeters, et al., Vibration-based bearing fault detection for operations and maintenance cost reduction in wind energy, Renewable Energy (2017), http://dx.doi.org/10.1016/j.renene.2017.01.056

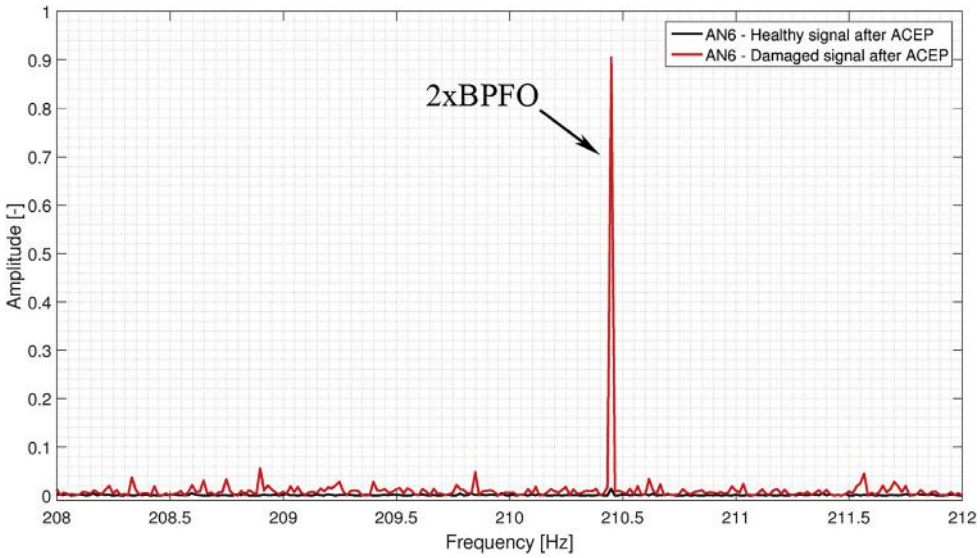

Fig. 17. Zoom of envelope spectrum of AN6 acceleration signal around the second BPFO harmonic of the ISS-B&C bearings for the healthy case (*black*) and damaged case (*red*). (For interpretation of the references to colour in this figure legend, the reader is referred to the web version of this article.)

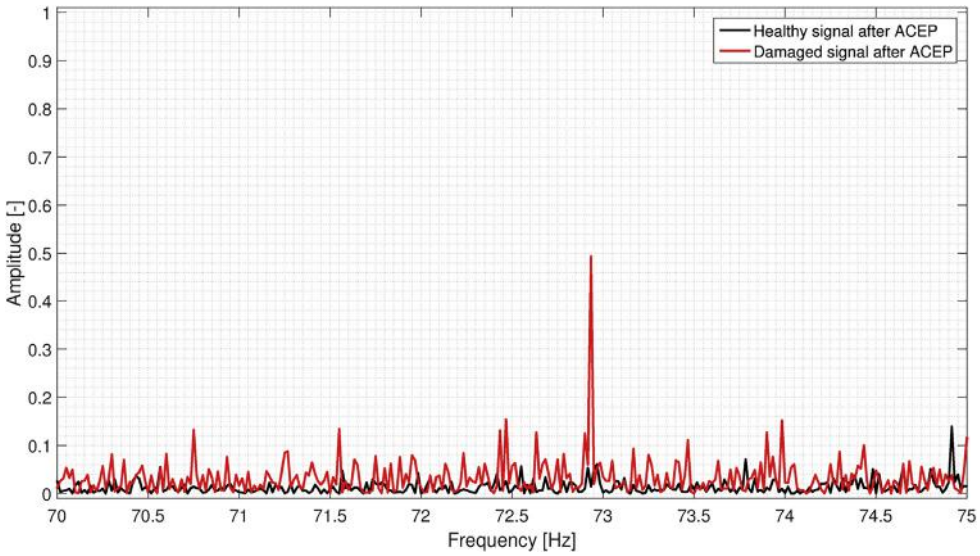

Fig. 18. Zoom of envelope spectrum around 72.94 Hz, the BPFI of the ISS upwind bearing, after bandpass filtering with center frequency 10 kHz and bandwidth 1 kHz.

The complex vibration signal consists of multiple deterministic signal components at various frequencies as well as noise. It was found that a simple autoregressive model fails to fit the deterministic signal part properly enough to effectively pre-whiten the signal for bearing fault detection. Attempts to optimize the model order as a function of kurtosis did not improve the results either. While not tested on this data, the SANC and DRS method would have to take care in their choice of a proper signal delay. The correlation length of the bearing fault signals has to be smaller than the delay, while the correlation length of the discrete content should be longer. There is however no guarantee this is the case, making the results possibly unreliable. The cepstrum editing procedure does not have these drawbacks or dependencies. No choice of delay or model order has to be made and the method only requires one step without having to iterate over all the present shafts or gears. The main parameter that can be changed in the CEP method is the number of samples to put to zero in the liftering step. This amount of samples depends on the sample rate and the length of the signal and could potentially be calculated automatically as well. For the examined data it was found that varying this parameter did not change the results as long as the amount of samples was not chosen to be excessively large.

Overall it is found that the proposed combination of techniques increases the detection rate and sensitivity to faults while remaining robust to non-impulsive background noise and easy to implement. However, care should be taken in the presence of impulsive noise or other impulsive disturbances. Since the use of the kurtogram relies on the use of kurtosis as a means of determining the appropriate band-pass filter, this technique can be affected by impulsive disturbances and thus present misleading results. In contrast, cepstral editing is unaffected by these disturbances since randomly occurring impulses mainly lead to an overall increase of all frequencies in the spectrum and thus does not change the harmonic structure. Potential future improvements can include tackling the reduction of background noise by implementing a noise reduction technique as well as implementing

Please cite this article in press as: C. Peeters, et al., Vibration-based bearing fault detection for operations and maintenance cost reduction in wind energy, Renewable Energy (2017), http://dx.doi.org/10.1016/j.renene.2017.01.056

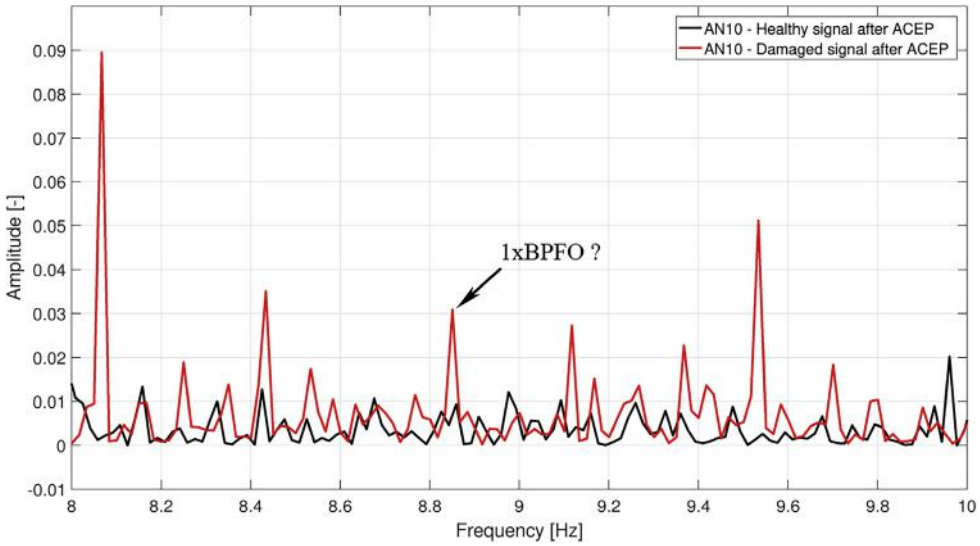

Fig. 19. Zoom of the envelope spectrum around 8.85 Hz, the BPFO of the PLC upwind bearing.

Table 5
Overview of the results of the bearing fault vibration analysis.

Bearing label	Fault type	Detection confidence level	Observations
HS-SH downwind bearings (*HSS-B & C*)	BPFI FTF	High High	Fundamental frequencies and harmonics are clearly visible, even for full bandwidth demodulation
IMS-SH downwind bearings (*ISS-B & C*)	BPFO	High	Full bandwidth shows even BPFO harmonics clearly, kurtogram is necessary for finding fundamental frequency
Planet carrier upwind bearing (*PLC-A*)	BPFO	Low	Envelope spectrum peak corresponding to BPFO is too small to make any claims about fault presence
IMS-SH upwind bearing (*ISS-A*)	BPFI	Medium	After bandpass filtering, the fundamental frequency is visible

alternatives to the kurtogram for increasing the robustness to impulsive noise. Possible other extensions might include defining thresholds for fault detection and identification, determining the fault size and estimating the remaining useful lifetime of components.

While the CEP method does remove discrete frequency content, it still does not remove any other masking cyclostationary content. The person who does the analysis of the envelope spectra still has to take into account the possible presence of other cyclostationary sources, as was observed during the analysis of the NREL data due to the multitude of faults. In summary, the cepstrum editing procedure proves to be a very easy-to-use and helpful tool in filtering out the influence of the deterministic content and increasing the sensitivity of the envelope analysis for bearing faults.

6. Conclusions

This paper assesses the performance of a combination of techniques and prominently of the automated cepstrum editing procedure (ACEP) for a real-world example, more in particular for the data provided by the *National Renewable Energy Laboratory* (NREL). This data is made available in the context of the *wind turbine gearbox condition monitoring round robin study* and is very well documented. Other research teams investigated this data as well, providing an interesting and useful background for comparison of the obtained results. Analysis of the results shows that the cepstrum editing procedure is a promising and straightforward preprocessing tool to use for removal of masking high-energy deterministic signal content. Comparison of the envelope spectra before and after application of the ACEP method reveal that the envelope spectra of the residual signal after ACEP is much less populated with interfering discrete frequency peaks and much easier to interpret and detect possible faults. As such, the ACEP method fits in well in automated vibration analysis schemes since it increases the confidence with which faults are detected.

Acknowledgement

The authors would like to sincerely thank the National Renewable Energy Laboratory for providing the well-documented data sets and for organizing the wind turbine gearbox condition monitoring round robin study, which produced a lot of interesting and priceless research content. Lastly, we would like to thank the agency for Innovation by Science and Technology for supporting the SBO HYMOP project. The National Renewable Energy Laboratorys GRC is funded by the U.S. Department of Energy under Contract No.DE-AC02-05CH11231.

Nomenclature

BPFO	Ball Pass Frequency of Outer race
BPFI	Ball Pass Frequency of Inner race
FTF	Fundamental Train Frequency
BSF	Ball Spin Frequency
LSS	Low-Speed Shaft
ISS	Intermediate-Speed Shaft
HSS	High-Speed Shaft
CRB	Cylindrical Roller Bearing
fcCRB	full-complement Cylindrical Roller Bearing
TRB	Tapered Roller Bearing
A	Upwind
B&C	Downwind

Please cite this article in press as: C. Peeters, et al., Vibration-based bearing fault detection for operations and maintenance cost reduction in wind energy, Renewable Energy (2017), http://dx.doi.org/10.1016/j.renene.2017.01.056

PLC	Planet carrier
ACEP	Automated Cepstrum Editing Procedure
NREL	National Renewable Energy Laboratory
DTF	Dynamometer Test Facility
SS	Spectral Subtraction
FFT	Fast Fourier Transform
IFFT	Inverse Fast Fourier Transform
E	Expectation operator
std	Standard deviation operator

References

[1] J. Helsen, Y. Guo, J. Keller, P. Guillaume, Experimental investigation of bearing slip in a wind turbine gearbox during a transient grid loss event, Wind Energy 19 (12) (2016) 2255–2269.

[2] M.I. Blanco, The economics of wind energy, Renew. Sustain. Energy Rev. 13 (6) (2009) 1372–1382.

[3] Y. Feng, Y. Qiu, C.J. Crabtree, H. Long, P.J. Tavner, Use of scada and cms signals for failure detection and diagnosis of a wind turbine gearbox, in: European Wind Energy Conference and Exhibition 2011, EWEC 2011, Sheffield, 2011, pp. 17–19.

[4] P. Bangalore, Load and Risk Based Maintenance Management of Wind Turbines, Chalmers University of Technology, 2014. Ph.D. thesis.

[5] J. Helsen, C. Devriendt, W. Weijtjens, P. Guillaume, Experimental dynamic identification of modeshape driving wind turbine grid loss event on nacelle testrig, Renew. Energy 85 (2016) 259–272.

[6] B.P. Graney, K. Starry, Rolling element bearing analysis, Mater. Eval. 70 (1) (2012) 78.

[7] X. Gong, W. Qiao, Current-based mechanical fault detection for direct-drive wind turbines via synchronous sampling and impulse detection, IEEE Trans. Ind. Electron. 62 (3) (2015) 1693–1702.

[8] X. Liu, Z. Gao, Robust finite-time fault estimation for stochastic nonlinear systems with brownian motions, J. Frankl. Inst..

[9] F.P.G. Márquez, A.M. Tobias, J.M.P. Pérez, M. Papaelias, Condition monitoring of wind turbines: techniques and methods, Renew. Energy 46 (2012) 169–178.

[10] J. Antoni, R. Randall, Unsupervised noise cancellation for vibration signals: part ii a novel frequency domain algorithm, Mech. Syst. Signal Process. 18 (1) (2004) 103–117.

[11] W. Wang, Autoregressive model-based diagnostics for gears and bearings, Insight-Non-Destructive Test. Cond. Monit. 50 (8) (2008) 414–418.

[12] R. Randall, N. Sawalhi, M. Coats, A comparison of methods for separation of deterministic and random signals, Int. J. Cond. Monit. 1 (1) (2011) 11–19.

[13] B. Kilundu, A.P. Ompusunggu, F. Elasha, D. Mba, Effect of parameters setting on performance of discrete component removal (dcr) methods for bearing faults detection, in: Proceedings of the European Conference of the Prognostics and Health Management (PHM) Society, Nantes (France), 8th-10th July, 2014, 2014.

[14] J. Helsen, G. De Sitter, P.J. Jordaens, Long-term monitoring of wind farms using big data approach, in: 2016 IEEE Second International Conference on Big Data Computing Service and Applications (BigDataService), IEEE, 2016, pp. 265–268.

[15] J. Antoni, Fast computation of the kurtogram for the detection of transient faults, Mech. Syst. Signal Process. 21 (1) (2007) 108–124.

[16] M. Zhao, J. Lin, X. Xu, Y. Lei, Tacholess envelope order analysis and its application to fault detection of rolling element bearings with varying speeds, Sensors 13 (8) (2013) 10856–10875.

[17] F. Combet, L. Gelman, An automated methodology for performing time synchronous averaging of a gearbox signal without speed sensor, Mech. Syst. Signal Process. 21 (6) (2007) 2590–2606.

[18] Q. Leclere, H. André, J. Antoni, A multi-order probabilistic approach for instantaneous angular speed tracking debriefing of the cmmno 14 diagnosis contest, Mech. Syst. Signal Process. 81 (2016) 375–386.

[19] N. Sawalhi, R.B. Randall, D. Forrester, Separation and enhancement of gear and bearing signals for the diagnosis of wind turbine transmission systems, Wind Energy 17 (5) (2014) 729–743.

[20] G. Dalpiaz, R. Rubini, G. D'Elia, M. Cocconcelli, F. Chaari, R. Zimroz, W. Bartelmus, M. Haddar, Advances in condition monitoring of machinery in non-stationary operations, in: Proceedings of the Third International Conference on Condition Monitoring of Machinery in Non-stationary Operations CMMNO, Springer, 2013.

[21] R.B. Randall, N. Sawalhi, A new method for separating discrete components from a signal, Sound Vib. 45 (5) (2011) 6.

[22] A.P. Ompusunggu, Automated cepstral editing procedure (acep) as a signal pre-processing in vibration-based bearing fault diagnostics, in: International Conference of Surveillance, 8, 2015.

[23] Y. Lu, P.C. Loizou, A geometric approach to spectral subtraction, Speech Commun. 50 (6) (2008) 453–466.

[24] S. Kamath, P. Loizou, A multi-band spectral subtraction method for enhancing speech corrupted by colored noise, in: IEEE International Conference on Acoustics Speech and Signal Processing, vol. 4, Citeseer, 2002, 4164–4164.

[25] L. Zhen, H. Zhengjia, Z. Yanyang, W. Yanxue, Customized wavelet denoising using intra-and inter-scale dependency for bearing fault detection, J. Sound Vib. 313 (1) (2008) 342–359.

[26] S. Sheng, Wind Turbine Gearbox Condition Monitoring Round Robin Study–vibration Analysis, 2012. Tech. rep., NREL Report No. TP-5000-54530, available at: http://www.nrel.gov/publications/.

[27] H. Luo, C. Hatch, M. Kalb, J. Hanna, A. Weiss, S. Sheng, Effective and accurate approaches for wind turbine gearbox condition monitoring, Wind Energy 17 (5) (2014) 715–728.

[28] J. Sheldon, G. Mott, H. Lee, M. Watson, Robust wind turbine gearbox fault detection, Wind Energy 17 (5) (2014) 745–755.

[29] D. Siegel, W. Zhao, E. Lapira, M. AbuAli, J. Lee, A comparative study on vibration-based condition monitoring algorithms for wind turbine drive trains, Wind Energy 17 (5) (2014) 695–714.

[30] Z. Zhang, A. Verma, A. Kusiak, Fault analysis and condition monitoring of the wind turbine gearbox, IEEE Trans. Energy Convers. 27 (2) (2012) 526–535.

[31] P. Tamilselvan, P. Wang, S. Sheng, J.M. Twomey, A Two-stage Diagnosis Framework for Wind Turbine Gearbox Condition Monitoring, 2013, p. 21. IJPHM Special Issue on Wind Turbine PHM (Color).

Please cite this article in press as: C. Peeters, et al., Vibration-based bearing fault detection for operations and maintenance cost reduction in wind energy, Renewable Energy (2017), http://dx.doi.org/10.1016/j.renene.2017.01.056